Thermoelectric properties of BiOCu1-xMxSe (M = Cd and Zn)

Article

Accepted Version

Thermoelectric Properties of $BiOCu_{1-x}M_xSe$ (M = Cd and Zn)

Son D. N. Luu[1] and Paz Vaqueiro[1,2*]

1. Institute of Chemical Sciences, Heriot-Watt University, Edinburgh, EH14, 4AS, UK
2. Department of Chemistry, University of Reading, Whiteknights, Reading RG6 6AD

Email: p.vaqueiro@reading.ac.uk

Abstract

Doping of BiOCuSe at the copper site with divalent cadmium and zinc cations has been investigated. Analysis of the powder X-ray diffraction data indicates that the ZrCuSiAs structure of BiOCuSe is retained up to substitution levels of 10 and 5 at.% for Cd^{2+} and Zn^{2+}, respectively. Substitution of monovalent Cu^{+} with divalent Cd^{2+} or Zn^{2+} leads to an increase in the magnitude of the electrical resistivity and the Seebeck coefficient. All synthesized materials behave as p-type semiconductors.

1. Introduction

Layered oxychalcogenides with the general formula ROTmCh (R = La, Ce, Nd, Pr, Bi; Tm = Cu, Ag and Ch = S, Se, Te) [1, 2, 3,4, 5] have attracted considerable interest due to their optoelectronic properties, as many of them are transparent p-type semiconductors [6]. These materials crystallise in the ZrCuSiAs structure, which consists of alternating fluorite and antifluorite layers (Figure 1), and are isostructural to the newly discovered superconducting oxypnictides LnOFePn (Ln = La, Pr, Ce, Sm; Pn = P and As) [7]. Very recently, it has been reported that two members of the oxychalcogenide family, BiOCuTe and BiOCuSe, exhibit promising thermoelectric properties at temperatures suitable for waste heat recovery [8, 9]. Their remarkable thermoelectric performance arises from a combination of very low thermal conductivities (κ) with reasonable values of the Seebeck coefficient (S) and the electrical conductivity (σ). This leads to promising values of the thermoelectric figure of merit (ZT), which is defined by $ZT = S^2\sigma T/\kappa$ and is related to the efficiency of thermoelectric energy recovery [10]. It has been suggested that these oxychalcogenides behave as "natural superlattices", which are layered materials in which slabs with excellent electronic transport properties are combined with a second type of slab which serves as a phonon scatterer, to reduce the thermal conductivity [11]. Other thermoelectric materials have been recently reviewed [12].

Recently, it has been shown that aliovalent substitution at the Bi^{3+} site in BiOCuSe can lead to p-type thermoelectric materials with an excellent performance [9, 13,14,15, 16]. For instance, high values of the thermoelectric figure of merit, ZT, have been obtained by doping with Sr^{2+} (ZT = 0.76 at 873 K) [9], Ca^{2+} (ZT= 0.8 at 773 K) [13], Pb^{2+} (ZT = 0.65 at 673 K)[14] and Mg^{2+} (ZT = 0.74 at 923 K) [15]. Doping with divalent Ba^{2+} ions at the Bi^{3+} site, combined with a reduction in grain sizes down to 200-

400 nm which decreases the thermal conductivity by ca. 40%, results in even higher ZT values of 1.1 at 923K [13]. Similar reductions in thermal conductivity have been found for ball milled BiOCuSe [17], suggesting that nanostructuring may be an effective approach to enhance the thermoelectric response of these materials. Instead of conventional solid-state synthesis and ball milling, a simple mechanical alloying process can be used to produce single phase nanocrystalline BiOCuQ (Q = Se, Te)[18]. Texturing of $Bi_{0.875}Ba_{0.125}OCuSe$ by hot forging also increases ZT up to 1.4 at 923K [19].

To date, efforts on modifying the electrical transport properties of BiOCuSe to improve its thermoelectric performance have been primarily focused on doping at the bismuth site. Isoelectronic substitution at the Se site, to form $BiOCuSe_{1-x}Te_x$, has been investigated by Liu *et. al.*, who have shown that it leads to improved electrical transport properties due to band gap tuning [21].To the best of our knowledge, the effect of aliovalent substitution at the copper site on the thermoelectric properties has not been investigated. However, it has been demonstrated that copper deficiency, which introduces holes into the conducting layer of BiOCuSe, results in a remarkable enhancement of the thermoelectric performance, with ZT reaching a value of 0.81 at 923 K [20]. In this paper, we report the effect of the partial substitution of Cu^+ by divalent cations (Cd^{2+} and Zn^{2+}) on the structure and transport properties of BiOCuSe.

2. Experimental procedure

2.1. Sample preparation

A series of polycrystalline $BiOCu_{1-x}M_xSe$ (M= Cd, and Zn; x= 0.05, 0.10, 0.15 and 0.20) compounds were synthesized by solid state reaction in evacuated and sealed silica tubes (< 10^{-4} Torr) from mixtures of Bi_2O_3 (99.99%, Sigma Aldrich), Bi (99.5%, Aldrich), Cu (99.5%, Johnson Matthey), CdO (≥99.99%, Aldrich) Zn (99%, Aldrich) and Se (99.99%, Aldrich). Each stoichiometric mixture was first heated up to 623 K for 20h and then up to 773 K for 10h with a 2 K min^{-1} ramp rate. A second annealing process at 873 K for a further 7h was carried out after regrinding the obtained powders. For electrical and thermal property measurements, the as-prepared powders were hot pressed into highly densified pellets (≥ 95% of theoretical density) at 853K and with a uniaxial pressure of 50 bars for 30 minutes under a N_2 flow.

2.2. Characterization and physical property measurements

2.2.1. Structural characterisation

Samples were characterized by powder X-ray diffraction (XRD) using a Bruker D8 Advance Powder X-ray diffractometer, operating with germanium monochromated $CuK_{\alpha1}$ radiation (λ = 1.54056 Å) and fitted with a LynxEye detector. Data were collected over a range of $5 \leq 2\theta/^{o} \leq 120$ for a period of 7 hours. Rietveld refinements were carried out using GSAS software [17].

2.2.2. Electrical transport measurements

The electrical resistivity of sample over the temperature range of $100 \leq T/K \leq 300$ was measured using a 4-probe DC technique. For each sample, a rectangular bar (~ 6 x 3 x 1 mm^3) was cut from a hot pressed pellet. Four 50μm silver wires were attached using silver paint and connections were made to a Keithley 2182 nanovoltmeter and a TTi QL564P power supply. The sample was mounted in an Oxford Instruments CF1200 cryostat connected to an ITC502 temperature controller. To measure the Seebeck coefficient over the same temperature range, the sample bar (~ 6 x 3 x 1 mm^3) was mounted on a copper holder, which incorporates a small heater (120 Ω strain gauge), located close to one end of the sample. The copper holder is attached to the hot stage of a closed-cycle refrigerator (DE-202, Advanced Research Systems), which is connected to a Lakeshore LS-331 temperature controller. Two 50μΩ copper wires were attached to the ends of the sample bar using silver paint and connections made to a Keithley 2182A nanovoltmeter. Two Au: 0.07% Fe vs. chromel thermocouples were placed at the hot and cold ends of the sample, and connected to a second Lakeshore LS-331 temperature controller. The Seebeck coefficient at a given temperature was determined by applying a temperature gradient, ΔT, across the sample and measuring the corresponding thermal voltage, ΔV. The slope of the line, $\Delta V/ \Delta T$, was used to determine the Seebeck coefficient.

For measurements above room temperature ($300 < T/K \leq 673$), the resistivity and Seebeck coefficient of each sample were measured simultaneously using a Linseis LSR-3 instrument (Germany).

2.2.3. Thermal transport measurements

An Anter FL3000 system was employed for measuring thermal diffusivity (α) and the heat capacity (C_p) of samples over a temperature range of $373 \leq T/K \leq 673$ in 50 K steps. Samples were hot pressed into highly densified pellets with a diameter of approximate 13 mm and a thickness of 1-2 mm. A graphite coating on the surface of pellet was applied to maximize heat absorption. The pellet was then loaded into the sample chamber which was purged with N_2 during the measurement. The thermal conductivity (κ) is calculated from the relationship $\kappa = \alpha C_p \rho$, where ρ is the sample density. A reference material, Pyroceram^{TM} 9606, of known heat capacity was used as a reference for the determination of the heat capacity of sample. The details of procedure of determination of the heat capacity are described in Ref. 21.

3. Results and discussion

3.1. Structural characterisation

Figure 2 shows selected powder X-ray diffraction patterns of the $BiOCu_{1-x}M_xSe$ (M = Cd, Zn) samples. Analysis of these data indicates that these materials crystallise in the ZrCuSiAs structure type (space group *P4*/mmm). Cd-containing samples with low dopant contents are single phases, while for the Zn-doped samples trace amounts of Bi_2O_2Se were detected. The maximum doping level was found at *ca.* x = 0.10 and 0.05 for Cd^{2+} and Zn^{2+}, respectively. Samples with larger values of x (Supplementary Information) contain significant amounts of impurities, which were identified by powder X-ray diffraction as CdSe and $Bi_{10}Cd_3O_{20}$ for Cd-containing samples and as Bi_2O_2Se for Zn-containing samples.

A representative Rietveld refinement is shown in Figure 3. The remaining refinements, together with tables of refined parameters, selected distances and angles are given in the Supplementary Information. As shown in Figure 4, in the single-phase region the *c* lattice parameter of $BiOCu_{1-x}Cd_xSe$ increases with increasing x. This expansion of the unit cell along the *c* axis might be related to the larger ionic radius of Cd^{2+} (109pm) when compared to that of Cu^+ (91pm) [13]. By contrast, substitution with Zn^{2+} results in a reduction in the lattice parameters (Supplementary Information), which may be related to the smaller ionic radius of Zn^{2+}(74pm). In all cases, there are only very small changes (~ ± 0.05 - 0.1%) in bond distance and angles with doping.

3.2. Electrical transport properties

The electrical conductivity of undoped BiOCuSe decreases with increasing temperature (Figures 5 and 6), indicating that this material exhibits a degenerate semiconducting behavior, in agreement with previous reports on BiOCuSe [14, 22]. In sharp contrast with doping at the Bi^{3+} site with divalent cations, which results in a significant enhancement of the electrical conductivity of BiOCuSe due to an increase in the concentration of holes [13,15,16,22], the substitution at the Cu^+ site with divalent ions leads to a major reduction in the electrical conductivity. With increasing levels of dopants, the electrical conductivity decreases in a systematic fashion, and the temperature dependence changes from that characteristic of a degenerate semiconductor to that expected for intrinsic behaviour. This may be indicative of a reduction in charge carrier concentration from the value of 1.1×10^{18} cm^{-3} previously found for undoped BiOCuSe [16]. Whilst Cd^{2+} and Zn^{2+} would be expected to act as n-type dopants, Cu^+ vacancies, which would act as acceptors, are known to form easily in this family of oxychalcogenides [20, 23], and this would lead to charge carrier compensation. Donor doping has been previously attempted in the related materials Sr_2MO_3CuS (M = Zn, Ga, In), which also contain $[Cu_2Q_2]^{2-}$ antifluorite-type layers, and it was found that p-type behavior was retained [24]. This was attributed to charge carrier compensation due to the formation of Cu^+ vacancies in the $[Cu_2S_2]^{2-}$ layers [24].

For $BiOCu_{1-x}M_xSe$, the Seebeck coefficient of all doped samples remains positive, indicating that the electrical transport properties are still dominated by holes. This is consistent with the p-type semiconducting behavior normally found for this family of oxychalcogenides. With the exception of $BiOCu_{0.95}Cd_{0.05}Se$, doped samples exhibit higher Seebeck coefficients than that of undoped BiOCuSe. This would be consistent with a reduction in the charge carrier concentration on donor doping. For $BiOCu_{0.9}Cd_{0.10}Se$, a step change in the Seebeck coefficient occurs between 480 and 550 K (Figure 6). This behavior may be indicative of a phase transition. Variable-temperature powder X-ray diffraction measurements may be required to elucidate this.

There is excellent agreement between the low- and high-temperature values of the Seebeck coefficient. However, the low-temperature electrical conductivity data are affected by greater uncertainties in sample dimensions, as well as by the Peltier effect arising from the use of a constant DC current source [25]. For this reason, low-temperature conductivity data have not been used in a quantitative way for the calculation of the power factor, $S^2\sigma$. At temperatures above 300 K, the power factor of the doped samples (Figure 6) remains relatively unchanged with increasing temperature. However, its magnitude is significantly reduced when compared to that of BiOCuSe. This reduction arises from the extremely low electrical conductivities found for doped samples.

3.3. Thermal transport properties and figure of merit ZT

The thermal conductivity of the $BiOCu_{1-x}M_xSe$ samples as a function of temperature is shown in Figure 7(a). The total thermal conductivity of $BiOCu_{0.95}Zn_{0.05}Se$ is slightly higher than that of pristine BiOCuSe at the same temperature, whilst the Cd-doped samples exhibit lower thermal conductivities than that of BiOCuSe. The total thermal conductivity of BiOCuSe (as well as those of the doped samples) is significantly lower than that of Bi_2Te_3 (~ 2 W m^{-1} K^{-1})[26]; a behaviour which has been related to the two-dimensional nature of the structure of this material, which leads to scattering of phonons at the interfaces between chalcogenide and oxide layers [9,17]. The electronic and lattice contributions of the thermal conductivity were estimated using the electrical conductivity data in conjunction with the Wiedemann-Franz law, with a Lorenz constant of 2.45×10^{-8} W Ω K^{-2}. For BiOCuSe, the electronic contribution is around 4% of total thermal conductivity whilst for doped samples, the electronic contribution is below *ca*.0.1% of total thermal conductivity. This indicates that the charge carrier concentration of these doped samples is very low or their mobility is low.

The thermoelectric figure of merit of the donor-doped samples was reduced in comparison to that of BiOCuSe (Figure 7(b)). The low electrical conductivity of these materials has a deleterious effect on the thermoelectric performance, despite the low thermal conductivity found for these phases. The results presented here suggest that BiOCuQ may be difficult to dope n-type, due to charge carrier compensation arising from the presence of Cu^+ vacancies. The ease of formation of copper vacancies has been previously related to difficulties in n-type doping in other copper chalcogenides, in particular $CuGaSe_2$.[27] The lack of n-type BiOCuSe has significant implications for the construction of thermoelectric devices based on this family of oxychalcogenides, given that compatible n- and p-type materials are required.

4. Conclusions

In conclusion, the partial substitution of Cd^{2+} and Zn^{+2+} ions at Cu^+ sites of BiOCuSe was achieved by solid state synthesis. Powder X-ray diffraction data and Rietveld refinements show that $BiOCu_{1-x}M_xS$ phases with $x \leq 0.1$ for M = Cd and $x \leq 0.05$ for M=Zn, adopt a layered structure of the ZrCuSiAs type. For the Cd-containing samples, the lattice parameters increase with increasing doping content, in particular along the *c* axis. Results show that substitution at the Cu site leads to an increase in the magnitude of the electrical resistivity and the Seebeck coefficient, which may arise from charge carrier compensation due to the formation of Cu^+ vacancies.

Acknowledgements

We thank the Energy Technology Partnership and European Thermodynamics Ltd. for funding this project.

Supplementary Information: Powder X-ray diffraction data, Rietveld profiles, tables of refined parameters and selected distances and angles.

References

[1] Palazzi M Carcaly C and Flahaut J 1980 *J. Solid State Chem.* **35** 150-155

[2] Kusainova A M Berdonosov P S Akselrud L G Kholodkovskaya L N Dolgikh V A and Popovkin B A 1994 *J. Solid State Chem.* **112** 189-191

[3] Chan G H Den B Bertoni M Ireland J R Hersam M C Mason T O Van Duyne R P and Ibers J A 2006 *Inorg. Chem.* **45** 8264-8272

[4] Liu M L Wu L B Huang F Q Chen L D and Ibers J A 2007 *J. Solid State Chem.* **180** 62-69

[5] Hiramatsu H Yanagi H Kamiya T, Ueda K Hirano M, Hosono H 2008 *Chem. Mater.* **20** 326-334

[6] Ueda K Hiramatsu H Hirano M Kamiya T and Hosono H 2006 *Thin Solid Films* **496** 8-15

[7] Prakash J and Ganguli A K 2011 *Inorganica Chimica Acta* **372** 2–7

[8] Vaqueiro P Guelou G Stec M Guilmeau E and Powell A V 2013 *J. Mater. Chem. A* .**1** 520-523

[9] Zhao L D Berardan D Pei Y L Byl C Pinsard-Gaudart L and Dragoe N 2010 *App. Phys. Lett.* **97** 092118

[10] Rowe D M 2006 *Thermoelectrics Handbook: Macro to Nano* ed. D M Rowe (Boca Raton FL: CRC Press) Chapter 1

[11] Wan C Wang Y Wang N Norimatsu W Kusumoki M and Koumoto K 2010 *Sci. Technol. Adv. Mater.* **11** 044306

[12] Sootsman JR Chung DY Kanatzidis MG 2009 *Angew. Chem.* **48** 8616-8639

[13] Li F Wei T-R Kang F Li J-F 2013 *J. Mater. Chem A* **1** 11942-11949

[14] Luu S D N and Vaqueiro P 2013 *J. Mater. Chem. A* **1** 12270-12275

[15] Lan J-L Zhan B Liu Y-C Zheng B Liu Y Lin Y-H and Nan C-W 2013 *Appl. Phys. Lett.* **102** 123905

[16] Li J Sui J Pei Y Barreteau C Berardan D Dragoe N Cai W He J and Zhao L D 2012 *Energy Environ. Sci.* **5** 8543-8547

[17] Li F Li J-F Zhao L D Xiang K Liu Y Zhang B P Lin Y-H Nan C-W and Zhu H-M 2012 *Energy Environ. Sci.* **5** 7188-7195

[18] Pele V Barreteau C Berardan D Zhao L-D Dragoe N 2013 *J. Solid State Chem.* **203** 187-191

[19] Sui J Li J He J Pei Y-L Berardan D Wu H Dragoe N Cai W and Zhao L-D 2013 *Energy Environ. Sci.* **6** 2916-2920.

[20] Liu Y Zhao L-D Liu Y Lan J Xu W Li F Zhang B-P Berardan D Dragoe N Lin Y-H Nan C-W Li J-F and Zhu H 2011 *J. Am. Chem. Soc.***133** 20112-20115

[21] Gaal P S Apostolescu S P 2002 US Patent No. US 6,375,349.

[22] Barreteau C Bérardan D Amzallag E Zhao L D Dragoe N 2012 *Chem. Mater.* **24** 3168-3178

[23] Pitcher M J Smura C F. Clarke S J 2006 *Inorg. Chem.* **48** 9054-9056

[24] Ueda K Hirose S Kawazoe H Hosono H 2001 *Chem. Mater.* **13** 1880-1883

[25] Nolas G S Sharp J Goldsmid H J 2001 Thermoelectrics: Basic Principles and New Materials Developments, Springer, Berlin Heidelberg

[26] Scherrer H Scherrer S 1995 CRC Handbook of Thermoelectrics, Ed. D.M. Rowe, CRC Press, Boca Raton, FL, Chapter 19

[27] Persson C Zhao Y-J Lany S Zunger A 2005 *Phys Rev. B* **72** 035211

Figure captions

Figure 1	View of the crystal structure of ROTmCh (R = La, Ce, Nd, Pr, Bi; Tm = Cu, Ag and Ch = S, Se, Te).
Figure 2	Powder X-ray diffraction patterns of $BiOCu_{1-x}M_xSe$ (M = Cd, Zn).
Figure 3	Rietveld refinement using powder X-ray diffraction data for $BiOCu_{0.95}Cd_{0.05}Se$ (R_{wp}=10.71%). Key: observed data (red crosses); difference curve (blue line); calculated pattern (green line) and reflection positions (pink markers).
Figure 4	Lattice parameters as a function of composition for $BiOCu_{1-x}Cd_xSe$.
Figure 5	Temperature dependence of the electrical properties of $BiOCu_{1-x}M_xSe$ over the temperature range $100 \leq T/K \leq 300$: (a) Electrical conductivity (σ); and (b) Seebeck coefficient (S).
Figure 6	Temperature dependence of the electrical properties of $BiOCu_{1-x}M_xSe$ over the temperature range $300 < T/K < 673$: (a) Electrical conductivity (σ); (b) Seebeck coefficient (S) and (c) power factor ($S^2\sigma$).
Figure 7	Temperature dependence of (a) thermal conductivity (κ) and (b) figure of merit (ZT) of $BiOCu_{1-x}M_xSe$.

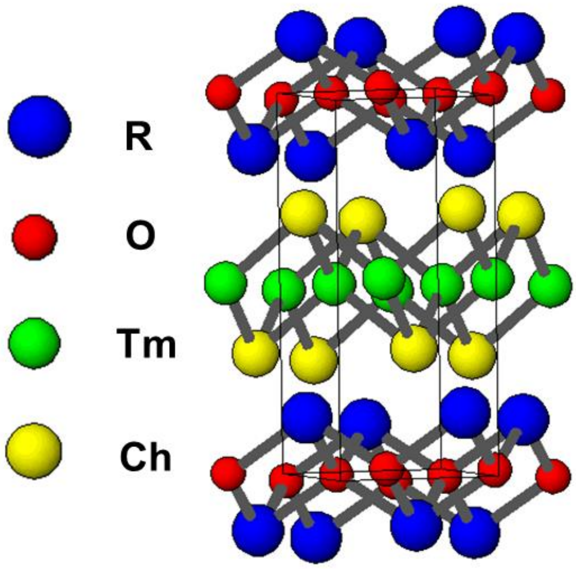

Figure 1

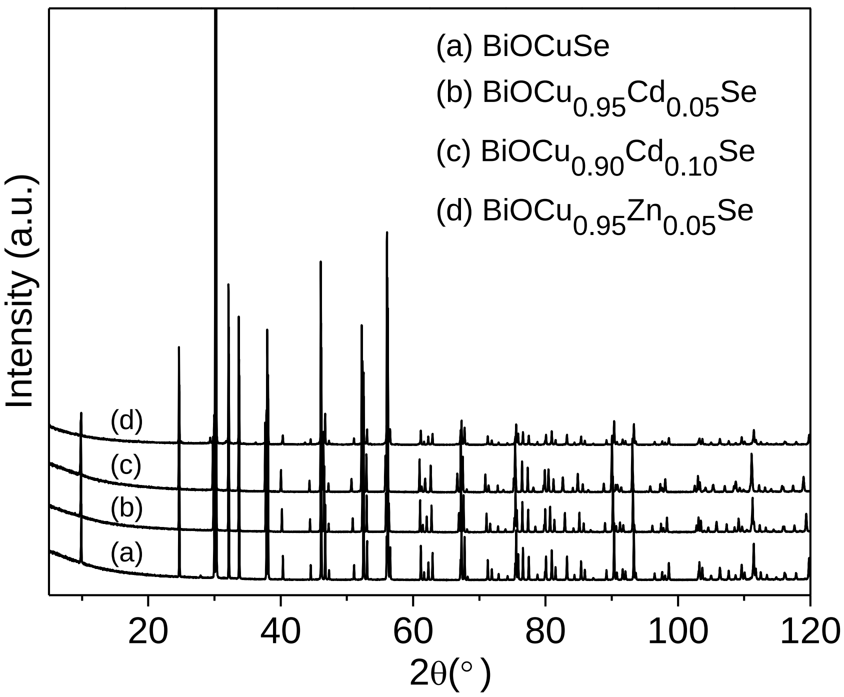
(a) BiOCuSe
(b) BiOCu0.95Cd0.05Se
(c) BiOCu0.90Cd0.10Se
(d) BiOCu0.95Zn0.05Se
Intensity (a.u.)
(d)
(c)
(b)
(a)
20
40
60
80
100
120
2θ(°)

Figure 2

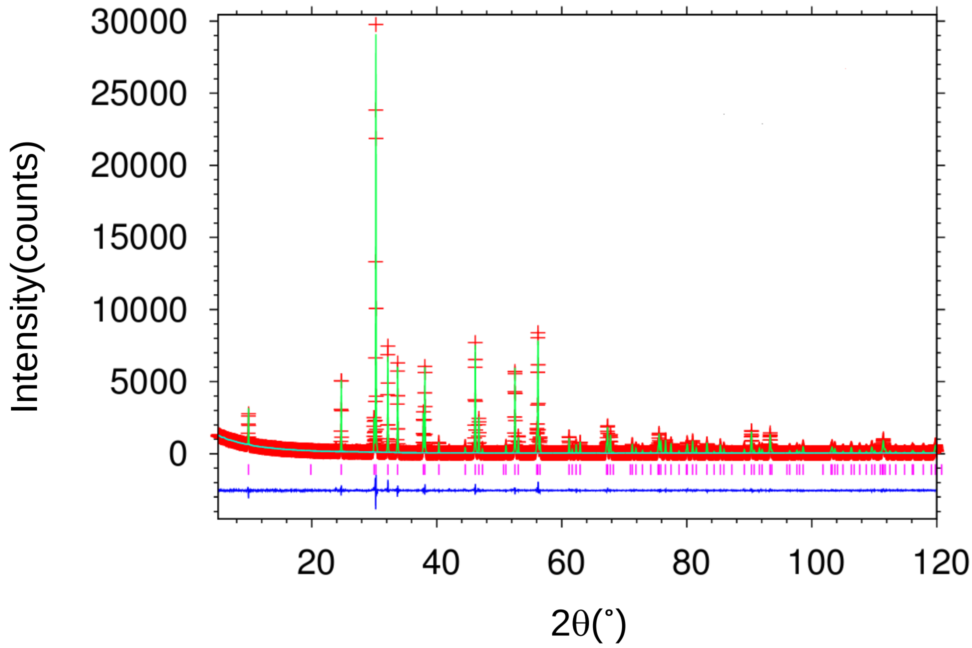
30000
25000
20000
15000
10000
5000
0
Intensity(counts)
20
40
60
80
100
120
2θ(˚)

Figure 3

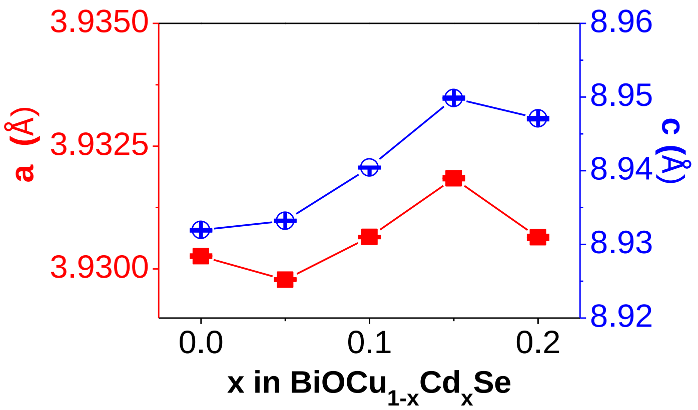
3.9350
3.9325
3.9300
a (Å)
8.96
8.95
8.94
8.93
8.92
c (Å)
0.0
0.1
0.2
x in BiOCu$_{1-x}$Cd$_x$Se

Figure 4

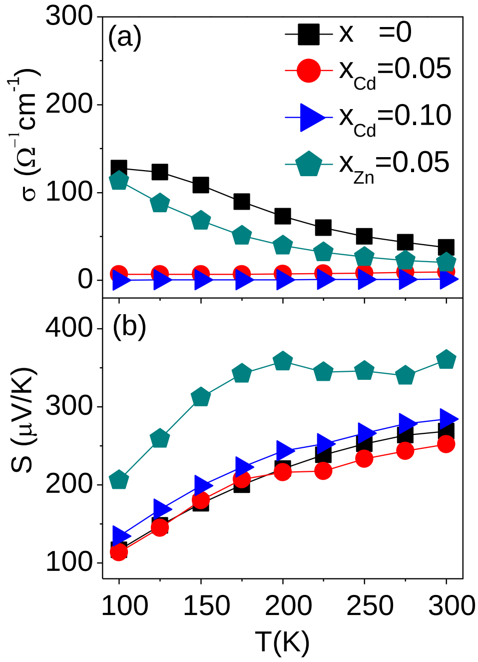
(a)
x =0
x_Cd=0.05
x_Cd=0.10
x_Zn=0.05
σ (Ω⁻¹cm⁻¹)
300
200
100
0
(b)
S (μV/K)
400
300
200
100
100
150
200
250
300
T(K)

Figure 5

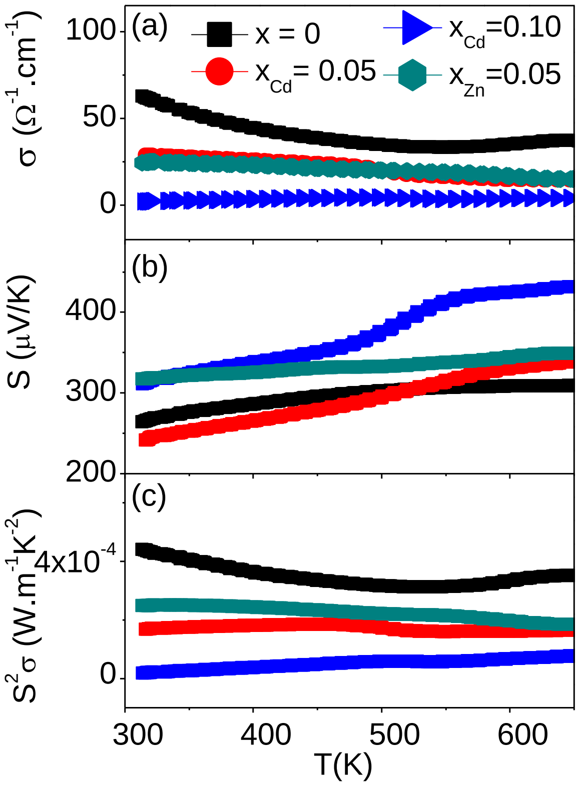

(a)
x = 0
x_{Cd}= 0.05
x_{Cd}=0.10
x_{Zn}=0.05
σ (Ω^{-1}.cm^{-1})
100
50
0
(b)
S (μV/K)
400
300
200
(c)
$S^2\sigma$ (W.m^{-1}K^{-2})
4x10^{-4}
0
300
400
500
600
T(K)

Figure 6

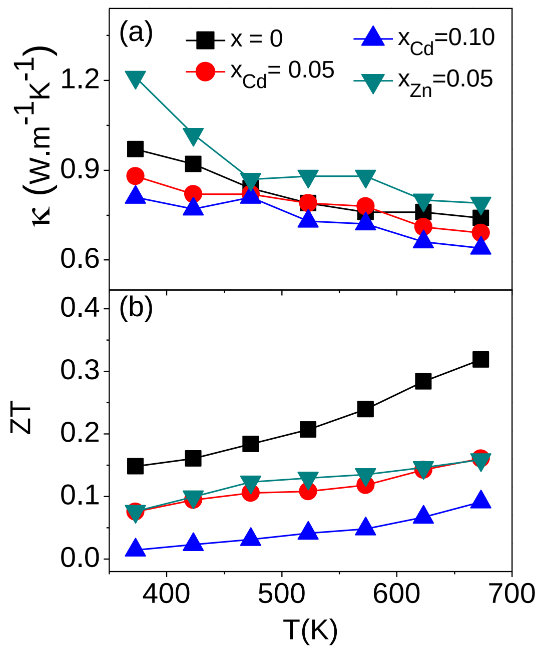

(a)
x = 0
x_Cd= 0.05
x_Cd=0.10
x_Zn=0.05
κ (W.m-1K-1)
1.2
0.9
0.6
(b)
0.4
0.3
0.2
0.1
0.0
ZT
400
500
600
700
T(K)

Figure 7